

MODELING OF MICRO-EXPLOSION FOR MULTICOMPONENT DROPLETS

Yangbing Zeng and Chia-Fon Lee
Department of Mechanical and Industrial Engineering
University of Illinois at Urbana-Champaign

INTRODUCTION

Micro-explosion refers to the fragmentation of liquid droplets due to violent internal gasification. It has strong potential in improving engine performance since it can be used to promote the atomization of heavy fuels by adding certain amounts of light fuels. With the aid of micro-explosion, the initial drop size can be relatively larger and thus the spray can penetrate further while maintaining a similar lifetime.

In recent 30 years, extensive experimental studies have been performed to understand the vaporization and combustion behavior of isolated droplets undergoing micro-explosion under combustion environment. In contrast, numerical efforts on micro-explosion are very limited. Several studies [1, 2] have been performed to analyze whether micro-explosion is possible by examining whether the temperature somewhere in the droplet interior reaches the superheat limit. Razzaghi [3] developed a model determining when micro-explosion occurs by tracking two time scales. One is the Rayleigh-Taylor stability time scale for a free falling droplet subject to the gravitational force. The other is the time scale for a perturbation to propagate from the interface to the equator. If the first one is larger than the second one, then breakup occurs.

This paper presents a numerical study on micro-explosion. From a theoretical point of view, the occurrence of micro-explosions for multicomponent droplets is primarily caused by the finite speed of mass diffusion within the droplet, and four steps are important for modeling micro-explosions, namely 1) tracing the evolution of temperature and mass fraction profiles inside the droplet, 2) identifying bubble generation, 3) tracing bubble growth, and 4) identifying explosion. In this study, the first and third steps are accompanied by a thermal description for a bubble-droplet system, the bubble generation is given by a homogeneous nucleation theory, and explosion is considered as the result of the breakup due to bubble growth. The model details are given in the subsequent section.

MATHEMATICAL MODEL

Thermodynamic Description

Depending on the vaporization history, one or two bubbles are generated before the occurrence of micro-explosion as observed by Wang et al. [4]. This study is limited to a one-bubble mode, and the bubble is assumed to be located at the droplet center. A schematic for this droplet containing a bubble is shown in Fig. 1. The effective diffusivity concept [5] is applied to reduce the problem to a one-dimensional description, and the interaction between the droplets and ambient gas is modeled using an integral approach. One-dimensional energy and mass conservation equations are used for the liquid film, while the pressure and temperature within the bubble are assumed to be uniform since in general the bubble growth velocity is much less than the corresponding sound speed within the bubble. It is also further assumed that the gas and liquid at the inner interface are in thermal and phase equilibrium. Bubble growth is determined by a modified Rayleigh equation [6].

For each liquid droplet, the initial temperature and composition are assumed to be uniform for simplicity. In contrast, the initial condition for the gas bubble is rather complicated. The two issues that need to be addressed are the onset of bubble generation and the initial size of the bubble, which will both be covered later.

Bubble Generation

This study focuses on the homogeneous nucleation that gives a lower bound for the onset of micro-explosion because the homogeneous nucleation in general requires higher superheat degree. Following Avedisian and Glassman's approach [7], the nucleation rate (number per volume per time) is given by

$$J = \Gamma \left[N_0 \exp\left(-\frac{\Delta A^*}{kT}\right) \right] k_f, \quad (1)$$

where N_0 is the molecular number density, k the Boltzman constant, ΔA^* the free energy of the critical nuclei, k_f the collision frequency, and Γ a constant between 0 and 1.

A variable N indicating the onset of homogeneous nucleation is defined as [8]

$$N(t) = \int_0^t \iiint J dV dt \quad (2)$$

N represents the number of active nuclei, and the onset of bubble generation is determined by

$$N(\tau_{bg}) = 1, \quad (3)$$

where τ_{bg} is the time for the onset of bubble generation. Whenever a bubble is generated, it is assumed that it is located at the center of the droplet and grows from its critical size.

Explosion

The breakup model proposed by Zeng and Lee [8] for a bubble-droplet system is used in this study to model the droplet explosion process. The breakup is assumed to occur when the disturbance grows larger than the product of the characteristic length of the system and a prescribed value. With this model, a breakup variable K is defined as

$$K(t) = \frac{R_{o0} e^{\int_0^t \omega dt}}{R_o - R_i}, \quad (4)$$

where ω is the disturbance growth rate, and the breakup occurs when

$$K(t_b) = K_{crit} \quad (5)$$

where t_b represents the breakup time. K_{crit} is the value of K at breakup, and this value can be optimized if comparable experimental data were available. In this study, $K_{crit} = 5$ is used to be consistent with existing experimental data. The normalized disturbance growth rate is determined by a linear stability analysis, and it is given by [8]

$$\left(\Delta - \Delta^2 - \psi_o \Delta\right) \bar{\omega}^2 + \left(-1 + \Delta^4 + \psi_o\right) We_o^{1/2} \bar{\omega} + 2\Delta^2 + 2\Delta^{-2} - 3\psi_i \frac{We_i}{Ma_i^2} \frac{\bar{\omega}}{\omega + 3We_i^{1/2}} \Delta^2 = 0, \quad (6)$$

where

$$\bar{\omega} = \sqrt{\frac{\rho_\ell R_i^{-3}}{\sigma}} \omega, \quad We_o = \frac{\rho_\ell V_o^2 R_i}{\sigma}, \quad We_i = \frac{\rho_\ell V_i^2 R_i}{\sigma}, \quad Ma_i = \frac{V_i}{c}, \quad \Delta = \frac{R_o}{R_i}, \quad \psi_o = \frac{\rho_{go}}{\rho_\ell}, \quad \psi_i = \frac{\rho_{gi}}{\rho_\ell}.$$

where ρ_ℓ the liquid density, R_i the bubble radius, σ the surface tension, V_o the droplet growth rate, V_i the bubble growth rate, c the sound speed in the bubble, ρ_o the ambient gas density, and ρ_i the bubble density. Three roots exist for the dispersion equation, and the root with the largest real part represents the disturbance growth.

The secondary droplets are assumed to have only a radial velocity component relative to the velocity of the parent drop. This velocity is determined by mass and momentum conservation, and it is given by [8]

$$V_b = \frac{3 R_i^2 V_i (R_o - R_i)}{R_o^3 - R_i^3}. \quad (7)$$

The Sauter-mean radius R_{32} of the secondary droplets is derived from mass and potential energy conservation before and after breakup, and it is given as

$$R_{32}^{-1} = B \frac{R_o^2 + R_i^2}{R_o^3 - R_i^3} + \left(\frac{3 R_i^4 (R_i^{-1} - R_o^{-1})}{2 R_o^3 - R_i^3} V_i^2 - \frac{V_b^2}{2} \right) \frac{\rho_\ell}{3\sigma}. \quad (8)$$

RESULTS AND DISCUSSIONS

The developed model was first validated by comparing predicted bubble growth and superheat limit with corresponding experimental data. The model was then used to analyze various parameters affecting the onset of homogeneous nucleation (nucleation is a prerequisite for micro-explosion) and the effects of micro-explosion.

Bubble Growth

Computations of water-bubble growth in an infinite media with a uniform temperature field were performed to validate the developed model. As suggested by Lee and Merte [9], a 10^{-4} K temperature perturbation is used at the first time step. Two cases of intermediate superheat degree under sub-atmospheric conditions are computed. The computational parameters and results are shown in Figs. 2 and 3. The results are also compared against measurements [10]. Satisfactory results are achieved for all three test cases. These results give us confidence in the developed model and the corresponding code.

Superheat Limit

The accuracy of the formula for evaluating the homogeneous nucleation rate is verified by comparing the computed superheat limit with the measured one. Avedisian and Glassman [7] have used Eq. (1) to predict the superheat limit for hydrocarbons. The superheat limit refers to the onset of violent boiling and is taken as the temperature when $J = 10^5/\text{cm}^3\text{-sec}$ computationally. Figure 4 shows the variation of superheat limit versus pressure for hexane, and the boiling temperature is also plotted. Excellent agreement between experiment and computation was obtained as expected. At lower pressures, the superheat limit requires a higher superheat degree (the difference between superheat limit and the boiling temperature). These results explain why homogeneous nucleation is easier at higher pressures since less superheat degree is required.

Pressure Effect

A set of computations were performed for a binary droplet at several different pressures. The simulated droplet consisted of 50% C_7H_{16} and 50% $\text{C}_{16}\text{H}_{34}$ in terms of mass and had an initial temperature of 293 K and an initial radius of 300 μm . The ambient temperature was set at 2300 K, which is roughly the adiabatic flame temperature of typical hydrocarbon fuels.

Figure 5 shows the temporal evolution of N defined by Eq. (2) ($N = 1$ indicates the onset of homogeneous nucleation). For convenience, N is set to 10^{-10} initially. It is noted that N increases very rapidly when there is a noticeable increase. Therefore, the critical value of N for the onset of homogeneous nucleation is not very important. Figure 6 shows the drop size at the onset of homogeneous nucleation for different pressures. At atmospheric pressure, N never changes noticeably until the droplet completely vaporizes. However, homogeneous nucleation becomes possible for pressures higher than atmospheric pressure, and it occurs earlier with increasing pressure [4]. A peak point for drop sizes at the onset of homogeneous nucleation was observed. With increasing pressure, the required superheat degree for homogeneous nucleation decreases, which favors homogeneous nucleation. On the other hand, the volatility differential between components decreases, which suppresses nucleation.

Composition Effect

Another set of computations were performed for $\text{C}_7\text{H}_{16}/\text{C}_{16}\text{H}_{34}$ droplets using different initial compositions. Again, the ambient temperature was set at 2300 K. The ambient pressure was set at 10 atm, and the droplet had an initial radius of 300 μm and an initial temperature of 293 K. Figure 7 shows the variation of drop sizes at the onset of homogeneous nucleation versus the mass fraction of the heavy component. The curve shows a parabola-like shape as observed in experiments [4], and the peak occurs at close to a mass fraction of 0.6. As the fraction of heavy component increases, the temperature that the droplet can reach increases, which favors onset of homogeneous nucleation. However, the amount of light component trapped inside the droplet decreases, which delays the onset of homogeneous nucleation.

Effect of Micro-Explosion

Computations were performed for binary droplets consisting of methanol and n-tetradecane. This is a fuel being used to model oxygenated diesel fuel. The computational parameters were chosen to simulate a typical diesel environment. An ambient pressure of 40 atm and a temperature of 842 K were used. Initially, the droplet had a temperature of 300 K, and a velocity of 60 m/sec. Since there is very few data on surface viscosity for mixtures of hydrocarbon and alcohol, a surface viscosity of 2.5×10^{-4} g/sec is used here. Figures 8 through 10 show the variation of the droplet squared radius versus time for three different compositions. The droplet has an initial radius of 20 μm . The results with and without consideration of micro-explosion are both plotted. The lifetime of the droplet with higher concentration of methanol is longer because the latent heat of methanol is much larger than that of n-tetradecane although its boiling point is lower. For all three cases, homogeneous nucleation occurs, and the subsequent micro-explosion shortens the droplet lifetime. For the case with an initial composition of 27% methanol in terms of mass, micro-explosion shortens the droplet lifetime by 20%. With increasing mass fraction of methanol, the micro-explosion occurs relatively earlier, and the effect of micro-explosion in turn becomes stronger. However, further increasing mass fraction of methanol delays the occurrence of micro-explosion. This is because that the maximum temperature (the boiling point at the droplet surface), that the droplet can reach, decreases with the increase of methanol content. The effect of droplet sizes on the occurrence of micro-explosion is shown in Figs. 9, 11 and 12. It was found that the micro-explosion occurs relatively earlier and the effect becomes stronger with increased drop sizes. This is because the mass fraction difference between the center and the surface is larger for larger droplets. Consequently, superheat region is easy to be built up resulting in a relatively earlier micro-explosion in terms of normalized time.

CONCLUSION

A numerical study of modeling micro-explosion for multicomponent droplets has been performed. The results can be summarized as follows.

(1) The formulated model for the thermodynamic description of the bubble-droplet system accurately predicted the bubble growth history over a wide range of superheat degrees and pressures.

(2) The defined variable N (number of active nuclei) is suitable for determining the onset of homogeneous nucleation, and the critical value of N for the onset of homogeneous nucleation is not very important since N increases very rapidly whenever there is a noticeable increase for N .

(3) The large volatility differences among components, and optimum composition favor micro-explosion. Higher pressure advances the onset of micro-explosion when the pressure is relatively lower, while it postpones the onset of micro-explosion when the pressure is relatively high.

(4) Occurrence of micro-explosion shortens the droplet lifetime, and this effect is stronger for larger droplets.

ACKNOWLEDGEMENTS

This work was supported in part by the National Science Foundation under grant No. CTS-9734402, with Farley Fisher as technical monitor, and by Ford Motor Company.

REFERENCES

1. C. K. Law, A Model for the Combustion of Oil/Water Emulsion Droplets, *Combustion Science and Technology*, Vol. 17, pp. 29-38, 1977.
2. C. K. Law and H. K. Law, A d^2 -Law for Multicomponent Droplet Vaporization and Combustion, *AIAA Journal*, Vol. 20, pp. 522-527, 1982.
3. M. Razzaghi, Droplet Size Estimation of Two-Phase Flashing Jets, *Nuclear Engineering and Design*, Vol. 114, pp. 115-124, 1989.
4. C. H. Wang, X. Q. Liu, C. K. Law, Combustion and Microexplosion of Freely Falling Multicomponent Droplets, *Combustion and Flame*, Vol. 56, pp. 175-197, 1984.

5. B. Abramzon and W. A. Sirignano, Droplet Vaporization Model for Spray Combustion Calculations, *International Journal of Heat and Mass Transfer*, Vol. 32, pp. 1605-1618, 1989.
6. L. E. Scriven, Dynamics of Fluid Interface, *Chemical Engineering Science*, Vol. 12, pp. 98-108, 1960.
7. C. T. Avedisian and I. Glassman, High Pressure Homogeneous Nucleation of Bubbles with Superheated Binary Liquid Mixtures, *ASME Journal of Heat Transfer*, Vol. 103, pp. 273-280, 1981.
8. Y. Zeng, "Modeling of Multicomponent Fuel Vaporization in Internal Combustion Engines", Ph. D. Thesis, University of Illinois at Urbana-Champaign, 2000.
9. H. S. Lee and H. Merte Jr., Spherical Vapor Bubble Growth in Uniformly Superheated Liquid, *International Journal of Heat and Mass Transfer*, Vol. 39, pp. 2427-2447, 1999
10. Y. C. Lien, Bubble Growth Rate at a Reduced Pressure, D. Sci. Thesis, MIT, 1969.

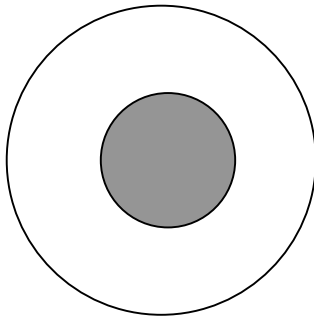


Fig. 1 Schematic of bubble/droplet

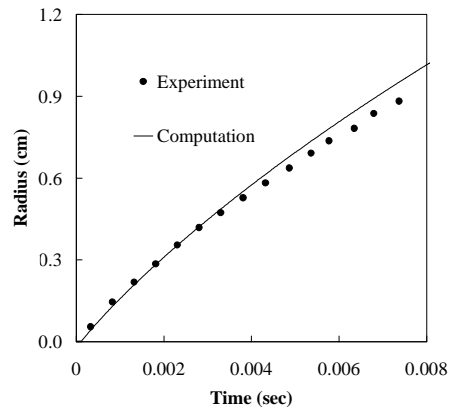


Fig. 2 Variation of bubble radius versus time (Case 1, $P = 12.6$ KPa, $\Delta T = 10.7$ K)

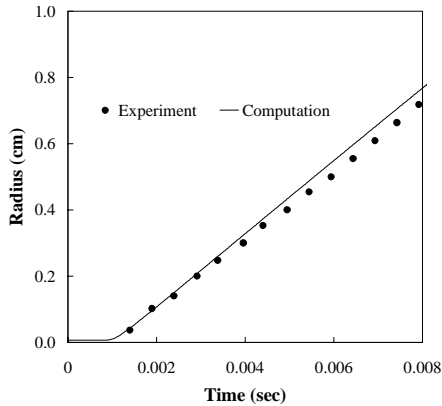


Fig. 3 Variation of bubble radius versus time (Case 3, $P = 1.26$ KPa, $T = 15.74$ K)

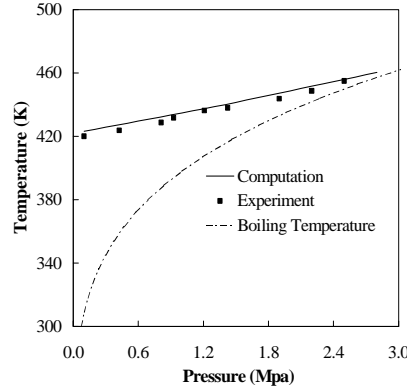


Fig. 4 Variation of superheat limit versus pressure for pentane

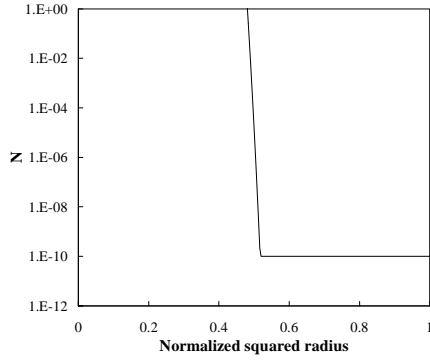


Fig. 5 Time resolution of N

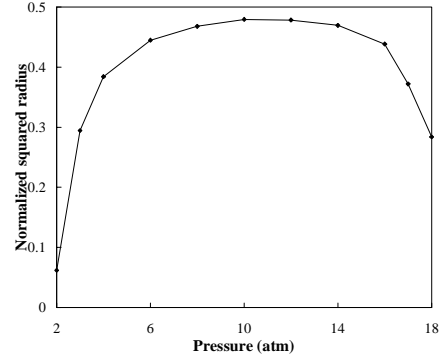


Fig. 6 Effect of pressure on onset of homogeneous nucleation

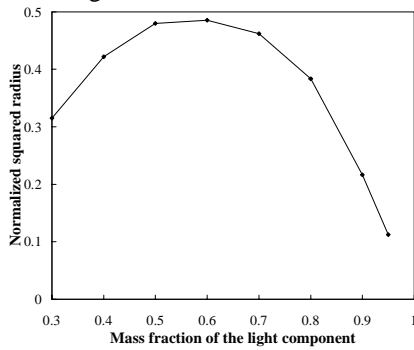


Fig. 7 Effect of drop initial composition

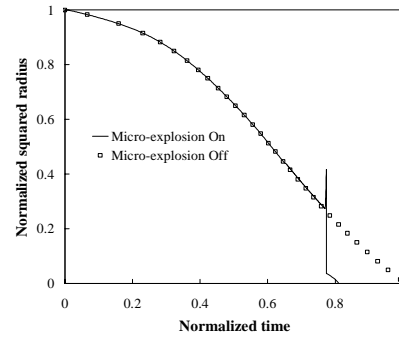


Fig. 8 Plot of droplet squared radius temporal history (27/73, lifetime without micro-explosion = 3.9 ms)

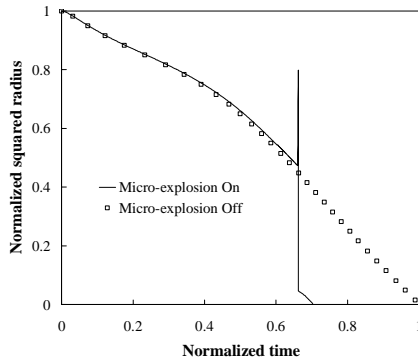


Fig. 9 Plot of droplet squared radius temporal history (50/50, 20 μm , lifetime without micro-explosion = 5.0 ms)

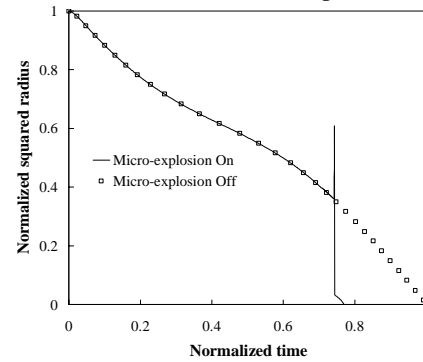


Fig. 10 Plot of droplet squared radius temporal history (70/30, lifetime without micro-explosion = 6.3 ms)

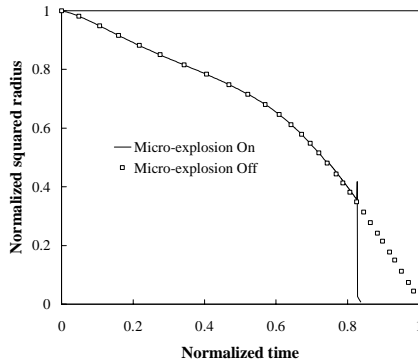


Fig. 11 Plot of droplet squared radius temporal history (10 μm , lifetime without micro-explosion = 2.1 ms)

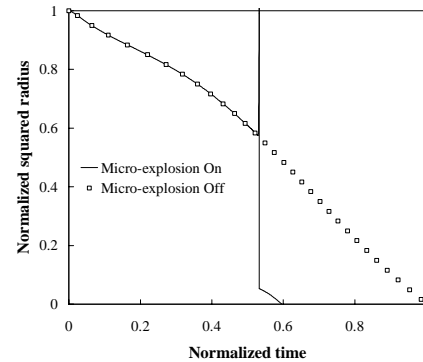


Fig. 12 Plot of droplet squared radius temporal history (30 μm , lifetime without micro-explosion = 9.5 ms)